



Research paper

Synthesis and photocatalytic activity of ultrafine Ag_3PO_4 nanoparticles on oxygen vacated TiO_2

Yang Li^a, Peifu Wang^a, Cunping Huang^b, Weifeng Yao^{a,*}, Qiang Wu^{a,*}, Qunjie Xu^{a,*}

^a Shanghai Key Laboratory of Materials Protection and Advanced Materials in Electric Power, College of Environmental & Chemical Engineering, Shanghai University of Electric Power, Shanghai, 200090, PR China

^b Aviation Fuels Research Laboratory, FAA William J. Hughes Technical Center, Atlantic City International Airport, NJ, 08405, USA

ARTICLE INFO

Article history:

Received 26 October 2016

Received in revised form

22 December 2016

Accepted 24 December 2016

Available online 26 December 2016

Keywords:

Silver phosphate

Photocatalysis

Water treatment

Oxygen vacated TiO_2

Ultrafine nanoparticles

ABSTRACT

Despite high activity for photocatalytic degradation of organic dyes from water, nanoscale Ag_3PO_4 photocatalyst particles are difficult to synthesize. As reported in literature, Ag_3PO_4 particle sizes for photocatalytic degradation of water pollutants are normally larger than 100 nm. This research reports a facile and reproducible method for the synthesis of the ultrafine and uniform Ag_3PO_4 nanoparticles loaded on the oxygen vacated TiO_2 ($\text{TiO}_2\text{-OV}$) with average particle size as small as 2.6 nm. All obtained Ag_3PO_4 particles can be completely loaded onto $\text{TiO}_2\text{-OV}$ support to form $\text{Ag}_3\text{PO}_4/\text{TiO}_2\text{-OV}$ composite photocatalysts. The prepared $\text{Ag}_3\text{PO}_4/\text{TiO}_2\text{-OV}$ photocatalyst exhibits much higher visible light photocatalytic activity than those of pure Ag_3PO_4 or $\text{Ag}_3\text{PO}_4/\text{TiO}_2$ photocatalysts for the degradation of rhodamine b (Rh B) and phenol in water. After depositing thin layers of AgI on Ag_3PO_4 ultrafine Ag_3PO_4 nanoparticles, the new $\text{AgI-Ag}_3\text{PO}_4/\text{TiO}_2\text{-OV}$ composite photocatalysts not only show much higher photocatalytic activity, but they are also more stable than pure Ag_3PO_4 catalyst. This new synthesis method will provide guidelines for the preparation of ultrafine nanoparticles and highly active photocatalysts for treatment of water pollution or production of hydrogen from water splitting/reducing.

© 2016 Elsevier B.V. All rights reserved.

1. Introduction

Water pollution has been a global concern over the past few decades and it continues to threaten both the quality of human lives and public health. Semiconductors, TiO_2 for example, are promising photocatalysts for the decontamination and purification of polluted water [1,2]. From a practical application viewpoint, however, pure TiO_2 is not a suitable photocatalyst because it is active only under ultraviolet (UV) light irradiation due to its wide band gap energy (3.2 eV). To better utilize sun radiation and improve water treatment efficiency the application of novel, visible-light-driven photocatalysts with high activity and stability is a must.

Ag-based photocatalysts, especially Ag_3PO_4 photocatalyst, have shown high photo-oxidative efficiency for organic dye decomposition from water [3–9]. For example, the visible light photocatalytic degradation rate of methylene blue in water over Ag_3PO_4 is ten times greater than those over BiVO_4 and commercial nitrogen-doped TiO_2 ($\text{TiO}_{2-x}\text{N}_x$) photocatalysts [6–8]. Despite their high

activity however, the low structural stability of Ag_3PO_4 photocatalysts strongly limits its practical application for water treatment. To address the low stability issue of Ag_3PO_4 , support materials are critical. Three-dimensional graphene [10], g-C₃N₄ [11,12], WS₂ [13], polyaniline (PANI) [14], hierarchical flower-like SnSe₂ [15], hierarchical In₂S₃ microspheres [16], macroporous WO₃ [17] and SAPO-34 zeolite [18,19] have been reported to improve the stability of Ag_3PO_4 . These studies confirm that support materials in Ag_3PO_4 /support composites can act as electron acceptors to suppress the charge recombination leading to the reduction of Ag_3PO_4 photocorrosion and finally to the enhancement of both the photocatalytic activity and the stability of Ag_3PO_4 . In addition to the supporting materials, integrating layers of a stable material onto the surface of Ag_3PO_4 particles can reduce the dissolution of Ag_3PO_4 in water, thus enhancing the stability of Ag_3PO_4 photocatalysts [8,11,14,20].

Currently, the extensively reported method for the preparation of Ag_3PO_4 based composites is the in-situ precipitation of Ag^+ and HPO_4^{2-} (or PO_4^{3-}) over a supporting material [10–19]. The great challenge for this method is that the current technological approach is unable to synthesize nanosized Ag_3PO_4 particles. The prepared Ag_3PO_4 particles are normally reported larger than 100 nm in Ag_3PO_4 /support composites. Fundamentally, the devel-

* Corresponding authors.

E-mail addresses: yaowefeng@shiep.edu.cn (W. Yao), qiangwu@shiep.edu.cn (Q. Wu), xuqunjie@shiep.edu.cn (Q. Xu).

opment of a facile process for depositing nanostructured Ag_3PO_4 over a supporting material is highly desirable.

In 2012 our research group reported a facile technology for the synthesis of $\text{Ag}_3\text{PO}_4/\text{TiO}_2$ composites with enhanced visible-light photocatalytic performance [21]. The $\text{Ag}_3\text{PO}_4/\text{TiO}_2$ composites are synthesized by electrostatically driven self-assembly between positively charged Ag^+ and negatively charged P25 TiO_2 in an aqueous solution with pH greater than 6. The results have shown that fine Ag_3PO_4 particles can be as small as 7 nm in diameter on the TiO_2 surface [21]. However, some very large Ag_3PO_4 particles (300–400 nm) (Fig. S1 of the Supporting Information) are occasionally observed in addition to the nanosized Ag_3PO_4 particles. The appearance of large Ag_3PO_4 particles can be ascribed to weak electrical attraction and uniform TiO_2 morphology. In summary of the literature search, a simple and direct process still remains attractive for the synthesis of nanosized and uniformly distributed Ag_3PO_4 particles over a supporting medium.

In this paper, a facile and reproducible method was successfully developed to prepare ultrafine Ag_3PO_4 nanoparticles with an average particle size as small as 2.6 nm. All prepared Ag_3PO_4 nanoparticles can be completely deposited onto oxygen vacated TiO_2 (TiO_2 -OV, P25) with effective visible light photocatalytic performance [22–25]. To the best of our knowledge, the preparation of such small Ag_3PO_4 nanoparticles has not been reported in literature. The visible-light-driven photocatalytic activities, together with the structural and physicochemical properties of the composites of ultrafine Ag_3PO_4 nanoparticles on TiO_2 -OV ($\text{Ag}_3\text{PO}_4/\text{TiO}_2$ -OV), were characterized using various technologies.

2. Experimental

2.1. Materials

Degussa P25 TiO_2 was purchased from Degussa, Hulls Corporation, Germany. Benzotrifluoride (BTF) with purity greater than 99% was purchased from Aladdin Industrial Corporation. Silver nitrate (AgNO_3), $\text{Na}_2\text{HPO}_4 \cdot 12\text{H}_2\text{O}$, benzyl alcohol (>99%) (BA), ammonium oxalate ($(\text{NH}_4)_2\text{C}_2\text{O}_4 \cdot \text{H}_2\text{O}$), *tert*-butyl alcohol (TBA, $(\text{CH}_3)_3\text{COH}$), 1,4-benzoquinone ($\text{C}_6\text{H}_4\text{O}_2$) were purchased from Sinopharm Chemical Reagent (Shanghai, China). Deionized water was supplied from local sources. All materials were used as received without further purification.

2.2. Synthesis

TiO_2 with oxygen vacancies (TiO_2 -OV) was prepared by using a previously reported method [22]. In a typical process, 1.0 g commercial Degussa P25 TiO_2 powder was added into a Pyrex glass bottle containing 60 mL BTF solvent and 8.0 mmol benzyl alcohol. The mixture was then irradiated under UV light for several hours using a 300 W Xe arc lamp (PLS-SXE 300, Beijing Perfectlight) with a band-passing filter (365 ± 15 nm). After UV-light irradiation, the produced yellow powder (TiO_2 -OV) was separated by centrifugation and washed with ethanol and deionized water several times.

The $\text{Ag}_3\text{PO}_4/\text{TiO}_2$ -OV composites were synthesized using an electrostatically driven method. In a typical process 0.4 g of synthesized TiO_2 -OV powder was added into 180 mL ethanol under ultrasonication. A stoichiometric amount of AgNO_3 was mixed with the TiO_2 -OV suspension under vigorous stirring for one hour. Under stirring, stoichiometric Na_2HPO_4 dissolved in 20 mL distilled water was then added dropwise into the above dispersion. The mixture was stirred for 5 h. The obtained precipitates were separated by centrifugation and washed several times with ethanol and deionized water. The prepared powders were then dried overnight in a vacuum oven at 60 °C. The entire synthesis was carried out in a dark

condition. Pure and unloaded Ag_3PO_4 was prepared under an identical experimental condition, but without the presence of TiO_2 -OV support material.

2.3. Characterizations of $\text{Ag}_3\text{PO}_4/\text{TiO}_2$ -OV composites

X-ray diffraction (XRD) experiments were carried out with a Bruker-D8 X-ray diffractometer using $\text{Cu-K}\alpha$ radiation. The scanning rate was 0.1 °/s. The accelerating voltage and the applied current were 40 kV and 40 mA, respectively. Scanning electron microscope (SEM) analysis was performed using a SU-1500 microscope (Hitachi, Japan). Transmission electron microscope (TEM) analysis was conducted on a JMT-2100F electron microscope. UV-vis diffusion reflectance spectra were recorded using a UV/VIS spectrometer (UV-2550, Shimadzu, Japan) and were then converted to absorption spectra using the standard Kubelka-Munk method. BaSO_4 was used as a reflectance standard in the UV-vis diffuse reflectance experiments. X-ray photoelectron spectroscopic (XPS) measurements were performed using an ultrahigh vacuum VG ESCALAB 210 electron spectrometer equipped with a multi-channel detector. The spectra were excited using $\text{Mg K}\alpha$ (1253.6 eV) radiation (operated at 200 W). Electron spin resonance (ESR) measurements to prove of oxygen vacancies in TiO_2 were operated on a Bruker EPR A300 spectrometer. The ESR analyses were carried out at room temperature under conditions of center field: 3506.65 G; modulation frequency: 100.00 kHz; microwave frequency: 9.8 GHz and power: 6.35 mW. The photoluminescence (PL) spectral analyses were detected on a spectrophotometer (RF-10A, Shimadzu, Japan) at the excitation wavelength of 365 nm. Photoelectrochemical measurements were performed in 0.1 M Na_2SO_4 electrolyte solution in a three-electrode quartz cell with a CHI 660 B electrochemical workstation. A saturated calomel electrode (SCE) and a large Pt foil were used as a reference electrode and a counter electrode, respectively. The $\text{Ag}_3\text{PO}_4/\text{TiO}_2$ -OV composite thin film on fluorine-doped tin oxide glass electrode was used as the working electrode for investigation.

2.4. Evaluation of photocatalytic activities of $\text{Ag}_3\text{PO}_4/\text{TiO}_2$ -OV photocatalysts

The photocatalytic activity of the $\text{Ag}_3\text{PO}_4/\text{TiO}_2$ -OV photocatalysts was evaluated based on the photocatalytic decomposition rates of aqueous rhodamine b (Rh B, a typical Azo dye) and phenol solutions at ambient temperature and atmospheric pressure. In a typical process, 0.1 g photocatalyst was suspended in an Rh B or a phenol (20 mg/L, 100 mL) aqueous solution. A 300W Xe arc lamp (Perfectlight Co., PLS-SXE300) equipped with a UV cutoff filter (UVCUT400, $\lambda > 400$ nm) was used as a light source for photocatalytic reactions. The illumination intensity was 140 mW·cm⁻². Prior to irradiation, the suspensions were stirred in darkness for 1 h to achieve equilibrium of pollutant adsorption-desorption on $\text{Ag}_3\text{PO}_4/\text{TiO}_2$ -OV photocatalysts. During photocatalytic reactions a certain suspension volume was sampled at selected time intervals and centrifuged to remove solid particles. The clear liquid was analyzed by recording the characteristic absorption peaks of Rh B at 554 nm and phenol at 280 nm using a spectrophotometer (UV-2550, Shimadzu Japan). The concentrations of the Rh B or phenol as functions of reaction time were used to determine dye degradation rates and the activities of $\text{Ag}_3\text{PO}_4/\text{TiO}_2$ -OV catalysts. The procedure for the addition of scavenging agents and $\cdot\text{OH}$ measurements followed the reported methods [26,27]. A total organic carbon analyzer (Multi N/C UV HS, Analytik Jena AG) was applied to analyse the mineralization degree of phenol.

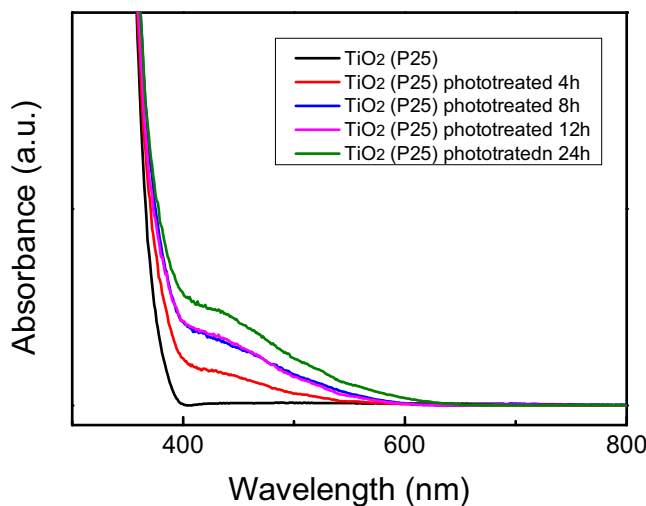


Fig. 1. UV-vis absorption spectra of TiO₂ (P25) and the TiO₂ with oxygen vacancies (TiO₂-OV) at different photo-treating time.

3. Results and discussion

3.1. Characterizations of TiO₂ with oxygen vacancies (TiO₂-OV)

TiO₂ with oxygen vacancies (TiO₂-OV) was successfully prepared using a benzyl alcohol assisted photo-treatment reported previously [22]. Fig. 1 shows the UV-vis absorption spectra of the prepared TiO₂-OV and the original TiO₂ powder samples (P25). The prepared TiO₂-OV samples exhibit absorption tails in the visible light region that are attributed to the presence of oxygen vacancies [22]. With an increase in the photo-treatment time, the light absorption intensity in the visible region increases significantly. This result indicates an extensive increase in oxygen vacancy sites on the surface of TiO₂ particles. The presence of oxygen vacancies in the prepared TiO₂-OV samples is further confirmed by the ESR spectroscopy (Fig. S2, Supporting Information). As shown in Fig. S2, the original TiO₂ sample (P25) does not show any paramagnetic signal prior to UV light treatment. In contrast, the prepared TiO₂-OV samples have an intense ESR signal at $g = 2.004$, which is ascribed to the single electrons trapping on the oxygen vacancies [22–25]. XPS spectral analysis indicates that the formation of oxygen vacancies does not accompany the generation of Ti³⁺ ions. As shown in Fig. S3 of the Supporting Information, the XPS spectrum of TiO₂-OV shows two main peaks at 458.5 and 464.2 eV, coinciding well with the position of Ti 2p_{3/2} and Ti 2p_{1/2} for Ti⁴⁺. The Ti 2p signals in the XPS spectrum are highly symmetric and no shoulder peaks are detected on the lower binding energy end of the Ti 2p spectrum (Fig. S3). These results indicate that the Ti³⁺ ions are not generated during the formation of oxygen vacancies on TiO₂ [28]. The O 1s spectrum of TiO₂-OV exhibited that the two characterized peaks at 529.8 and 531.1 eV are attributed to the Ti-O and hydroxyl species, respectively. These results agree very well with previous reports [22]. In this study, TiO₂ (P25) with 8 h photo-treatment was chosen as an oxygen vacated TiO₂ support (TiO₂-OV) for its relatively larger visible light absorption capacity.

3.2. Synthesis of Ag₃PO₄/TiO₂-OV composites

Ag₃PO₄/TiO₂-OV composites are synthesized by the electrostatically driven self-assembly between the positively charged Ag⁺ ions and the negatively charged TiO₂-OV particles (ESR results), followed by the addition of Na₂HPO₄ precipitant. The overall synthetic procedure of Ag₃PO₄/TiO₂-OV composites was illustrated in Scheme 1. When some oxygen atoms are removed from TiO₂ crys-

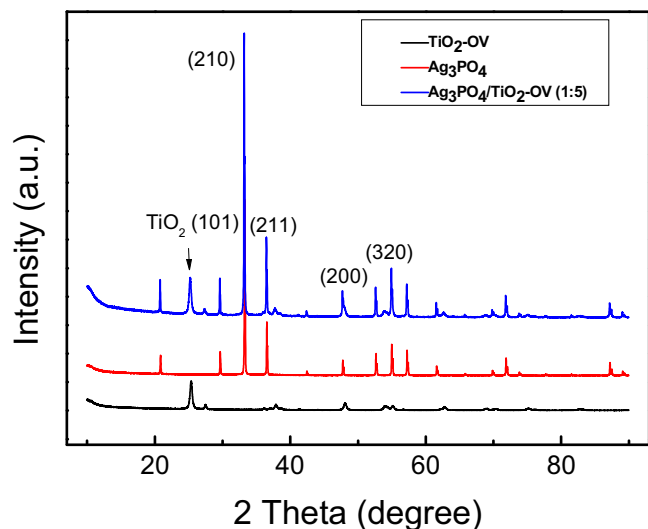
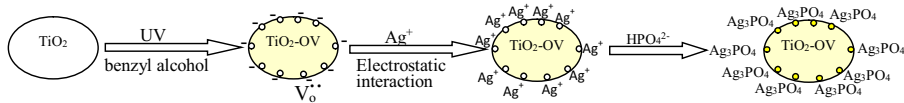


Fig. 2. XRD patterns of Ag₃PO₄, TiO₂-OV and Ag₃PO₄/TiO₂-OV (1:5) composites.

talline the -Ti-O-Ti-O-Ti- network will be distorted, generating high energy point defects on the TiO₂ surface. These atomic level and zero dimensional defects, along with relatively free movable electrons in the defects, can strongly attract Ag⁺ cations in the solution thereby forming very fine Ag₃PO₄ nuclei, which will then grow in-situ into Ag₃PO₄ nanocrystals in the presence of HPO₄²⁻ ions. Because oxygen vacancies in TiO₂ distribute evenly at an atomic level the formation of ultrafine Ag₃PO₄ nanoparticles also have a very uniform distribution (Fig. S8, Supporting Information). In this process the electrons located on the oxygen vacancy states can be partially neutralized by Ag⁺ ions. The small amount of adsorbed Ag⁺ ions may be reduced to form Ag metal particles.

The XPS spectra of the Ag species adsorbed on TiO₂-OV, prepared by Ag⁺ adsorption prior to the addition of Na₂HPO₄, show a significant Ag 3d signal, suggesting the efficient adsorption of Ag⁺ ions onto the surface of TiO₂-OV (Fig. S4, Supporting Information). The fitted Ag 3d peaks indicate that two Ag species coexist in Ag 3d_{5/2} and Ag 3d_{3/2} signals peaks at 367.7 and 368.7 eV can be assigned to Ag 3d_{5/2} and 373.7 and 374.9 eV for Ag 3d_{3/2}. XPS peaks at 367.7 and 373.7 eV can be attributed to Ag⁺ species, whereas the peaks at 368.7 and 374.9 eV can be ascribed to metal Ag particles. These results are in agreement with previous reports [29,30]. The observation of the metallic Ag suggests that a small amount of the adsorbed Ag⁺ cations on the surface of TiO₂-OV can be reduced to form elemental Ag atoms. Similar results can also be found for Pt and Au ions that could be reduced to metallic Pt and Au atoms on the surface of weakly reductive TiO₂ and WO₃. [31,32] Consistent with the XPS results, the reduced ESR signal at $g = 2.004$ of TiO₂-OV after Ag⁺ ion adsorption (Fig. S5, Supporting Information) also indicates the formation of Ag metal atoms on the surface of TiO₂-OV.

Fig. 2 shows the XRD patterns of prepared Ag₃PO₄, TiO₂-OV and Ag₃PO₄/TiO₂-OV composite photocatalyst with an Ag₃PO₄ to TiO₂-OV molar ratio of 1:5. All the diffraction peaks of Ag₃PO₄ correspond to the body-centered cubic (b.c.c) structure of Ag₃PO₄ (JCPDS NO.01-071-1836), while peaks of TiO₂-OV can be indexed as a mixture of the anatase and rutile TiO₂ (P25) (Fig. 2 and Fig. S6). The XRD patterns of Ag₃PO₄/TiO₂-OV composite match well with the polycrystalline structures of Ag₃PO₄ and TiO₂-OV, ruling out the involvement of a third phase. These results point to the formation of Ag₃PO₄/TiO₂-OV composite. However, the XRD patterns of prepared Ag₃PO₄/TiO₂-OV composite does not show any Ag metallic peaks. This result may indicate that metallic Ag particles on the surface of TiO₂-OV are either highly dispersed or amorphous or the mass concentration of Ag is at a very low



Scheme 1. Schematic pathways for synthesizing $\text{Ag}_3\text{PO}_4/\text{TiO}_2\text{-OV}$ composites.

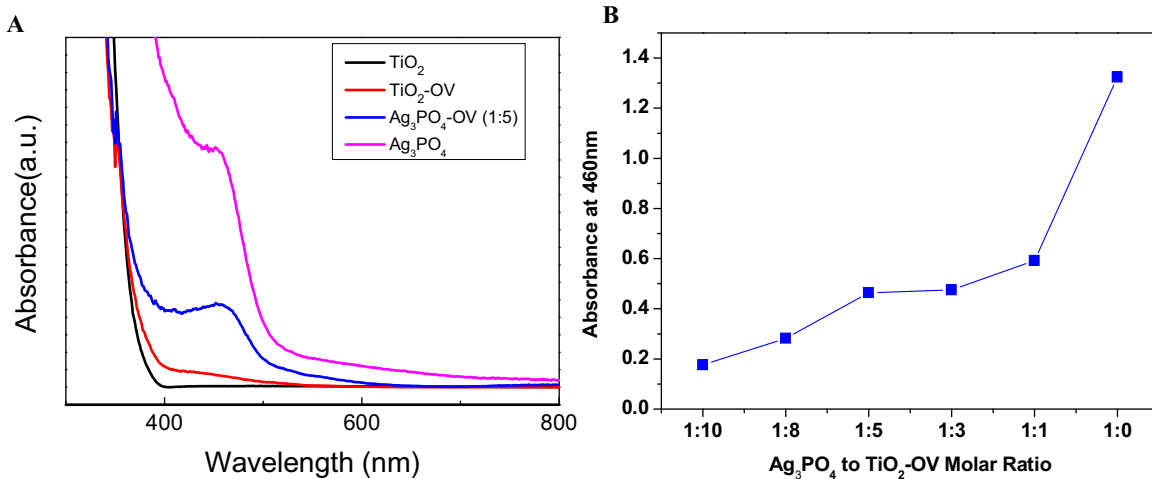


Fig. 3. UV-vis absorption spectra of (A) for TiO_2 (P25), $\text{TiO}_2\text{-OV}$, $\text{Ag}_3\text{PO}_4/\text{TiO}_2\text{-OV}$ (Ag_3PO_4 to TiO_2 molar ratio = 1:5) and Ag_3PO_4 ; (B) UV-vis spectral absorbance of different molar ratio $\text{Ag}_3\text{PO}_4/\text{TiO}_2\text{-OV}$ samples at 460 nm.

level. Fig. 3(a) shows the UV-vis absorption spectra of TiO_2 (P25), $\text{TiO}_2\text{-OV}$, Ag_3PO_4 and the $\text{Ag}_3\text{PO}_4/\text{TiO}_2\text{-OV}$ composites. The $\text{TiO}_2\text{-OV}$ sample exhibits an absorption tail of less than 500 nm in the visible light region, which is attributed to the oxygen vacancies on the surface of $\text{TiO}_2\text{-OV}$ [22–25]. The absorption band edge of $\text{TiO}_2\text{-OV}$ is located at approximately 376 nm, corresponding to the band gap energy of 3.3 eV, the same as that of the original TiO_2 (P25). In contrast, Ag_3PO_4 can absorb both UV light and visible light with wavelengths lower than 507 nm, corresponding to band gap energy of 2.45 eV. This result agrees with the light-absorption properties of Ag_3PO_4 reported by other groups [7]. For $\text{Ag}_3\text{PO}_4/\text{TiO}_2\text{-OV}$ nanocomposites, except for the characteristic absorption band edge (about 507 nm) of Ag_3PO_4 , a feature band edge (380 nm) of $\text{TiO}_2\text{-OV}$ appears in the UV light range, suggesting that Ag_3PO_4 and $\text{TiO}_2\text{-OV}$ form composites. The UV-vis absorption spectra of $\text{Ag}_3\text{PO}_4/\text{TiO}_2\text{-OV}$ nanocomposites with different Ag_3PO_4 to $\text{TiO}_2\text{-OV}$ molar ratios show that the absorbance at 460 nm for $\text{Ag}_3\text{PO}_4/\text{TiO}_2\text{-OV}$ composites increases consistently with the increase of the Ag_3PO_4 to $\text{TiO}_2\text{-OV}$ molar ratio (Fig. 3(b) and Fig. S7). It is evident therefore that Ag_3PO_4 content in the composites determines the visible light absorption capability of the $\text{Ag}_3\text{PO}_4/\text{TiO}_2\text{-OV}$ photocatalysts.

Fig. 4 shows the typical TEM and HRTEM images of prepared $\text{Ag}_3\text{PO}_4/\text{TiO}_2\text{-OV}$ (1:5) samples. Two distinct particles were found in TEM images Fig. 4(a). The large particles, with an average size of 25 nm, are assigned to the $\text{TiO}_2\text{-OV}$ (Degussa P25) particles [33]. The smaller particles, ranging from 1.7 to 5.0 nm (Fig. 4(b)), which are found on the surface of $\text{TiO}_2\text{-OV}$ particles, are Ag_3PO_4 nanocrystals. An HRTEM image of $\text{Ag}_3\text{PO}_4/\text{TiO}_2\text{-OV}$ (1:5) composite is shown in Fig. 4(c). The 0.245 nm lattice fringe spacing corresponds to {211} plane of b.c.c Ag_3PO_4 crystals. [34] The characteristic lattice fringes of 0.352 nm and 0.248 nm of $\text{TiO}_2\text{-OV}$ can be indexed as the {101} planes of anatase TiO_2 and rutile TiO_2 , respectively (Fig. 4(c)). Fig. 4(d) shows the energy-dispersive X-ray (EDS) patterns of $\text{Ag}_3\text{PO}_4/\text{TiO}_2\text{-OV}$ (1:5) composite. The signals from elemental Ag, P, Ti and O signals result from Ag_3PO_4 and $\text{TiO}_2\text{-OV}$. The EDS signals for C and Cu are mainly from the copper sub-

strate TEM sample holder. EDS results also confirm the formation of $\text{Ag}_3\text{PO}_4/\text{TiO}_2\text{-OV}$ composites.

TEM analyses for the $\text{Ag}_3\text{PO}_4/\text{TiO}_2\text{-OV}$ composites with various Ag_3PO_4 to $\text{TiO}_2\text{-OV}$ molar ratios are shown in Fig. S8. Results indicate that prepared Ag_3PO_4 particles on the surface of $\text{TiO}_2\text{-OV}$ are all in nanosized. Particle size of Ag_3PO_4 nanocrystals deposited on $\text{TiO}_2\text{-OV}$ does not change significantly when the molar ratio of Ag_3PO_4 to $\text{TiO}_2\text{-OV}$ decreases from 1:1 to 1:5. The average diameter of the prepared Ag_3PO_4 increases only from 2.6 to 3.1 nm. However, when the molar ratio of Ag_3PO_4 to $\text{TiO}_2\text{-OV}$ increases to 1:3 there are two kinds of Ag_3PO_4 nanoparticles which appear on the surface of $\text{TiO}_2\text{-OV}$. As shown in Fig. S8(B), there are many very small particles (~1 nm) present on the surface of the $\text{TiO}_2\text{-OV}$, and few relatively large particles (3–9 nm) with an average diameter of 5.5 nm (Fig. S8(b)). Upon further increasing the molar ratio of Ag_3PO_4 to $\text{TiO}_2\text{-OV}$ to 1:1 a few Ag_3PO_4 particles as large as 40 nm appeared along with some small Ag_3PO_4 nanoparticles with an average diameter of 4.3 nm (Fig. S8(A)). It is noteworthy that the average particle size of prepared pure Ag_3PO_4 without $\text{TiO}_2\text{-OV}$ support is approximately 250 nm with irregular spherical morphology (Fig. S9). These results indicate that $\text{TiO}_2\text{-OV}$ support plays an important role in controlling the size of the Ag_3PO_4 particles in the composites. The effect of the $\text{TiO}_2\text{-OV}$ support is attributed to the self-assembly of positively charged Ag^+ on negatively charged $\text{TiO}_2\text{-OV}$, driven by electrostatic interaction which hinders generation and controls the growth of Ag_3PO_4 seed particles [21] along with the higher defect energies of oxygen vacancies in TiO_2 .

3.3. Photocatalytic activities for the degradation of rhodamine B and phenol aqueous solutions

The photocatalytic behaviors of the $\text{Ag}_3\text{PO}_4/\text{TiO}_2\text{-OV}$ and pure Ag_3PO_4 were characterized via degradation of Rh B and phenol aqueous solutions. The photocatalytic reaction was carried out using visible light ($\lambda \geq 400$ nm) irradiation at room temperature. Fig. 5 (a) depicts the degradation of a 20 mg/L 100 mL aqueous Rh B solution based on its concentration changes over three photocat-

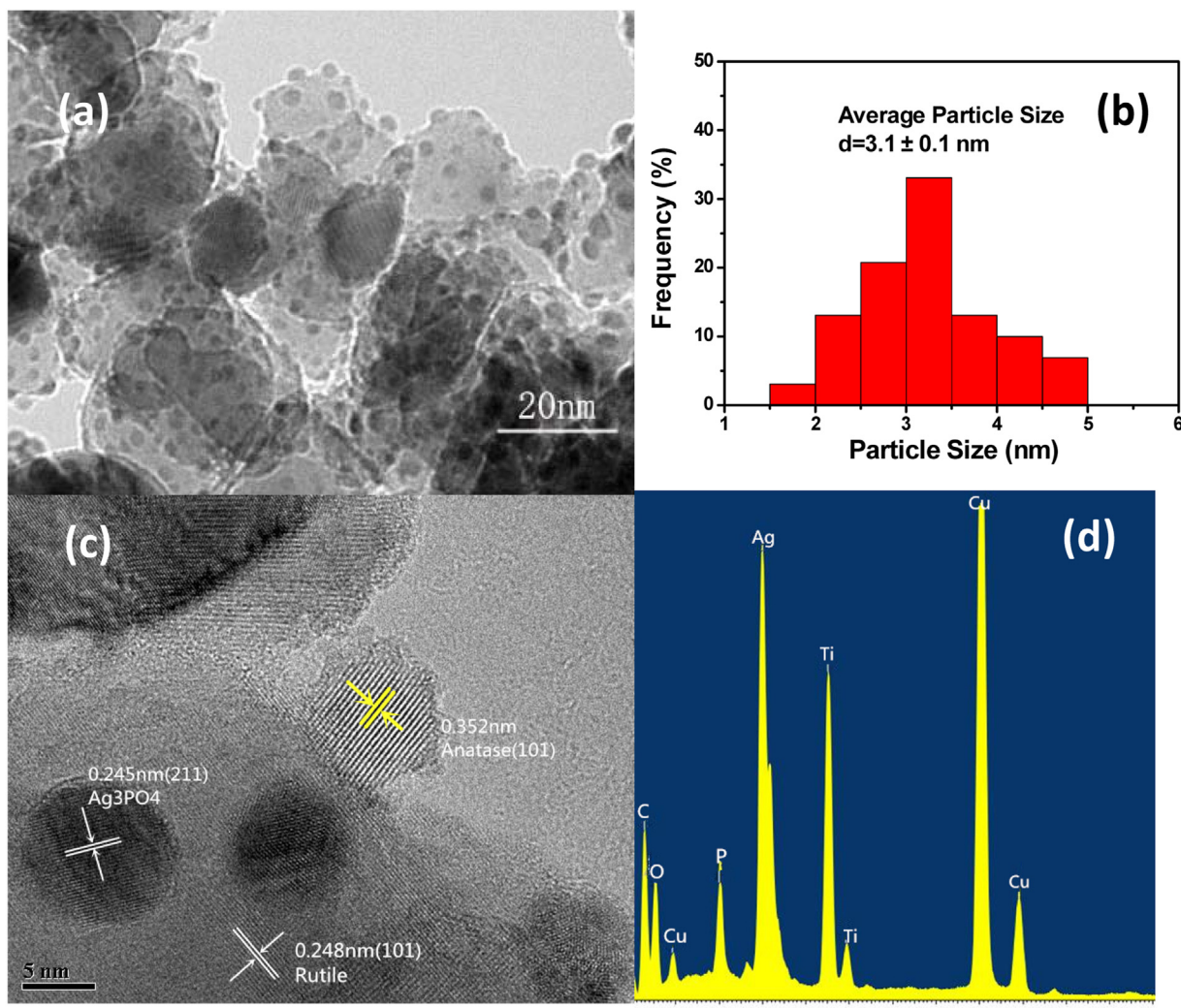


Fig. 4. Images of TEM (a), particle size distribution histograms (b), HRTEM (c), and EDX (d) of an $\text{Ag}_3\text{PO}_4/\text{TiO}_2$ -OV photocatalyst with Ag_3PO_4 to TiO_2 -OV molar ratio = 1:5.

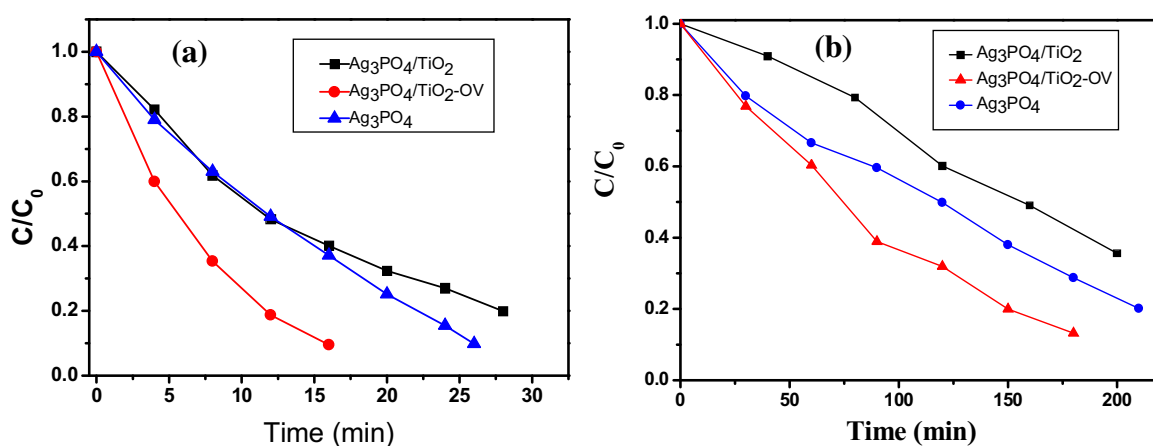


Fig. 5. Photocatalytic degradation of (a) rhodamine B (Rh B) and (b) phenol aqueous solutions (100 mL 20 mg/L) over 0.1 g of $\text{Ag}_3\text{PO}_4/\text{TiO}_2$ -OV (molar ratio = 1:5), $\text{Ag}_3\text{PO}_4/\text{TiO}_2$ (P25) (molar ratio = 1:5) and pure Ag_3PO_4 photocatalysts under visible light irradiation ($\lambda > 400$ nm).

alysts. The concentration of the aqueous Rh B solution decreases rapidly with $\text{Ag}_3\text{PO}_4/\text{TiO}_2$ -OV (1:5) nanocomposite. 90% of Rh B was photocatalytically degraded after 16 min of light irradiation. Pure Ag_3PO_4 required about 26 min for degrading the same amount of Rh B dye. $\text{Ag}_3\text{PO}_4/\text{TiO}_2$ (1:5) required about 28 min for 80% of Rh B

dye conversion. The kinetics of the photocatalytic reaction can be described using a pseudo-first-order reaction for low concentration of Rh B solutions:

$$\text{Rate} = -\ln(\text{C}_t/\text{C}_0) = kt$$

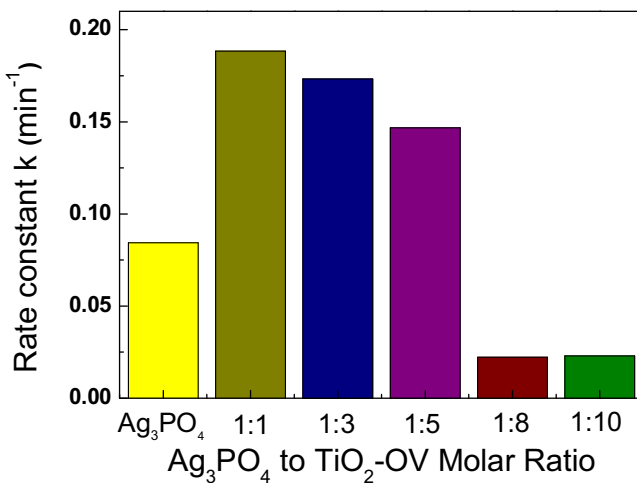


Fig. 6. Photocatalytic degradation rate constant (k , min^{-1}) for the photocatalytic degradation of rhodamine b (Rh B) aqueous solution over $\text{Ag}_3\text{PO}_4/\text{TiO}_2\text{-OV}$ with different Ag_3PO_4 to $\text{TiO}_2\text{-OV}$ molar ratios.

where C_0 and C_t are the Rh B concentrations at irradiation time $t=0 \text{ min}$ and $t=t \text{ min}$, respectively. k is the first order reaction rate constant (min^{-1}). The k for Rh B degradation over $\text{Ag}_3\text{PO}_4/\text{TiO}_2\text{-OV}$ (1:5), calculated based on a pseudo-first-order equation, is 0.27 min^{-1} , which is 4.8 times greater than that of $\text{Ag}_3\text{PO}_4/\text{TiO}_2$ (1:5) composites (0.056 min^{-1}). These results indicate that $\text{Ag}_3\text{PO}_4/\text{TiO}_2\text{-OV}$ nanocomposite exhibits a much higher photocatalytic activity for Rh B degradation than both pure Ag_3PO_4 and $\text{Ag}_3\text{PO}_4/\text{TiO}_2$ photocatalysts. Since the photocatalyst mass used for the reaction is the same (0.1 g) for all three catalysts, the mass percentage of silver for $\text{Ag}_3\text{PO}_4/\text{TiO}_2\text{-OV}$ (1:5) has been reduced from 77 wt.% for pure Ag_3PO_4 to 39 wt.% for $\text{Ag}_3\text{PO}_4/\text{TiO}_2\text{-OV}$ (1:5), but the rate constant of Rh B degradation over $\text{Ag}_3\text{PO}_4/\text{TiO}_2\text{-OV}$ (1:5) increases 3.4 times as compared with that of pure Ag_3PO_4 photocatalyst. This result indicates a significant cost reduction for Ag_3PO_4 based photocatalysts.

Fig. 5(b) shows similar results for the photodegradation of phenol in water over three photocatalysts. 61% of the phenol was photocatalytically degraded after 90 min reaction over $\text{Ag}_3\text{PO}_4/\text{TiO}_2\text{-OV}$ (1:5) nanocomposite. Pure Ag_3PO_4 photocatalyst required about 147 min and $\text{Ag}_3\text{PO}_4/\text{TiO}_2$ (1:5) took about 190 min to degrade 61% of the phenol. The mineralization of phenol was confirmed by the total organic carbon (TOC) analysis (Fig. S10, Supporting Information). These results also indicate that the photocatalytic activity of $\text{Ag}_3\text{PO}_4/\text{TiO}_2\text{-OV}$ (1:5) under visible light irradiation is much greater than that of both pure Ag_3PO_4 and $\text{Ag}_3\text{PO}_4/\text{TiO}_2$ (1:5) composite photocatalysts. The photodegradation of the colorless phenol suggests that the visible light photocatalytic activity of the $\text{Ag}_3\text{PO}_4/\text{TiO}_2\text{-OV}$ composite is not caused by photolytic dye degradation occasionally found for Azo dye under visible light irradiation, but rather is promoted via photocatalytic reactions over $\text{Ag}_3\text{PO}_4/\text{TiO}_2\text{-OV}$ catalysts.

The loading amount of Ag_3PO_4 over $\text{TiO}_2\text{-OV}$ can be optimized via photocatalytic activities of $\text{Ag}_3\text{PO}_4/\text{TiO}_2\text{-OV}$ composites for Rh B degradation. As shown in Fig. 6, the photocatalytic activities of $\text{Ag}_3\text{PO}_4/\text{TiO}_2\text{-OV}$ composites do not change significantly when the molar ratio of Ag_3PO_4 to $\text{TiO}_2\text{-OV}$ decreases from 1.0 (1:1) to 0.2 (1:5). Although the activity of $\text{Ag}_3\text{PO}_4/\text{TiO}_2\text{-OV}$ (1:5) is slightly lower than those of $\text{Ag}_3\text{PO}_4/\text{TiO}_2\text{-OV}$ (1:3) and $\text{Ag}_3\text{PO}_4/\text{TiO}_2\text{-OV}$ (1:1) composites, the mass percentage of silver for $\text{Ag}_3\text{PO}_4/\text{TiO}_2\text{-OV}$ (1:5) is much less than that for $\text{Ag}_3\text{PO}_4/\text{TiO}_2\text{-OV}$ (1:3) and $\text{Ag}_3\text{PO}_4/\text{TiO}_2\text{-OV}$ (1:1) composites. Based on the activity to cost ratio, $\text{Ag}_3\text{PO}_4/\text{TiO}_2\text{-OV}$ (1:5) photocatalyst is considered to be the most cost effective for Rh B degradation. Further decreasing the

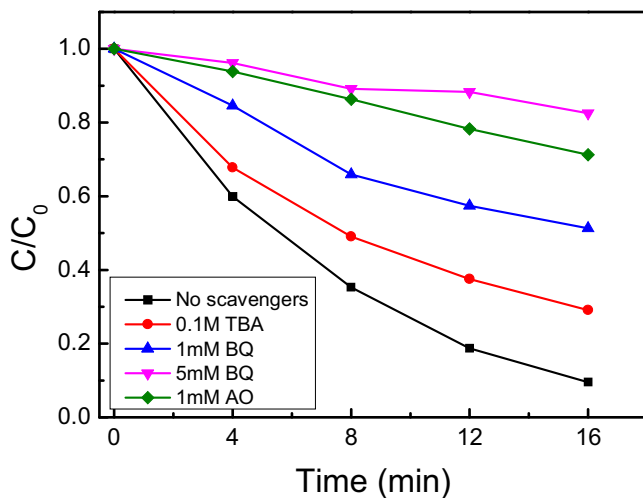


Fig. 7. Effect of various scavengers on the degradation of Rh B by $\text{Ag}_3\text{PO}_4/\text{TiO}_2\text{-OV}$ (1:5) under visible-light irradiation.

molar ratio of Ag_3PO_4 to $\text{TiO}_2\text{-OV}$ leads to a quick decrease in the photocatalytic activity (Fig. 6) as the concentration of Ag_3PO_4 in $\text{Ag}_3\text{PO}_4/\text{TiO}_2\text{-OV}$ becomes too low. In summary, both $\text{TiO}_2\text{-OV}$ support and the molar ratio of Ag_3PO_4 to $\text{TiO}_2\text{-OV}$ play crucially important roles in determining the photocatalytic performance of the composites.

3.4. Photocatalytic mechanism of $\text{Ag}_3\text{PO}_4/\text{TiO}_2\text{-OV}$ composites

The photodegradation mechanism of $\text{Ag}_3\text{PO}_4/\text{TiO}_2\text{-OV}$ composites was investigated by performing the radical-trapping experiments with different scavengers. Three chemicals, t-butyl alcohol (TBA, a $\cdot\text{OH}$ radical scavenger), ammonium oxalate (AO, a hole scavenger) and benzoquinone (BQ, an $\text{O}_2^{\cdot-}$ radical scavenger), were employed as scavengers for holes and radicals in trapping experiments. Fig. 7 shows that the addition of 1.0 mM BQ reduced the photocatalytic activity of Rh B degradation from 90% to 46% in 16 min. The photocatalytic degradation activity was further decreased from 90% to 20% after 16 min when a higher concentration of BQ (5 mM) was added to the 20 mM aqueous Rh B solution. A notable inhibitory effect on the degradation activity over the $\text{Ag}_3\text{PO}_4/\text{TiO}_2\text{-OV}$ composites was also observed when 1.0 mM AO was added to the Rh B solution, in which only 17% Rh B was degraded in 16 min under identical experimental conditions. In contrast, the presence of TBA (0.1 M) in the photocatalytic system does not significantly affect degradation of Rh B, where almost 70% Rh B was degraded in 16 min. These hole and radical trapping experiments suggest that photo-induced active hole scavengers and $\text{O}_2^{\cdot-}$ radicals, rather than $\cdot\text{OH}$ radicals, are the dominant species responsible for the highly efficient photocatalytic performance of $\text{Ag}_3\text{PO}_4/\text{TiO}_2\text{-OV}$ composites.

A possible photocatalytic mechanism of the composite photocatalyst $\text{Ag}_3\text{PO}_4/\text{TiO}_2\text{-OV}$ is proposed and shown in Fig. 8. As discussed above, a small number of adsorbed Ag^+ ions on the surface of $\text{TiO}_2\text{-OV}$ can be reduced to Ag° during the synthesis of $\text{Ag}_3\text{PO}_4/\text{TiO}_2\text{-OV}$ composites. This result can be verified by the reduced ESR intensity of $\text{TiO}_2\text{-OV}$ after Ag_3PO_4 deposition and the XPS spectrum of $\text{TiO}_2\text{-OV}$ with Ag species adsorption (Fig. S4 and Fig. S5). Based on this conclusion, the $\text{Ag}_3\text{PO}_4/\text{TiO}_2\text{-OV}$ can therefore be described as an $\text{Ag}_3\text{PO}_4/\text{Ag}/\text{TiO}_2\text{-OV}$ three component composite. In a photocatalytic process electron-hole pairs are generated when Ag_3PO_4 (conduction band: 0.45 V vs. NHE; valence band: +2.9 V vs. NHE) [7] is irradiated by visible light. A small number of photo-excited electron-hole pairs can also be generated by

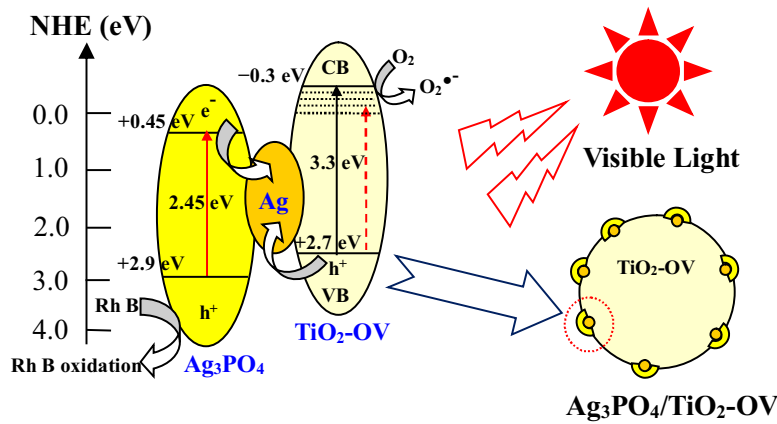


Fig. 8. Schematic representation of the enhanced photocatalytic efficiency of $\text{Ag}_3\text{PO}_4/\text{Ag}/\text{TiO}_2\text{-OV}$ photocatalyst.

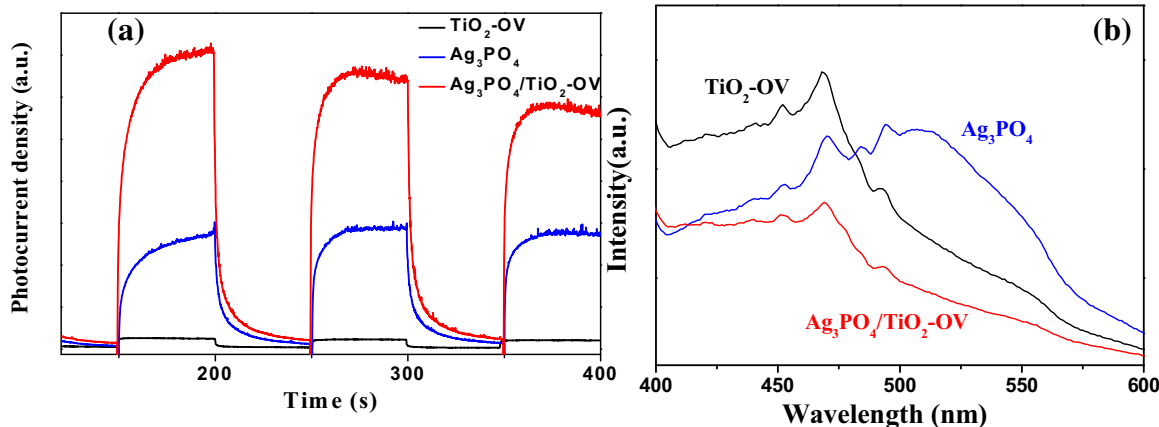


Fig. 9. Transient photocurrent response (a) and photoluminescence spectra (b) of the prepared $\text{TiO}_2\text{-OV}$, pure Ag_3PO_4 and $\text{Ag}_3\text{PO}_4/\text{TiO}_2\text{-OV}$ (1:5) photocatalysts.

$\text{TiO}_2\text{-OV}$, although $\text{TiO}_2\text{-OV}$ has a large band gap energy of 3.3 eV, with its potential of conduction band (-0.3 V vs. NHE) [35] and valence band ($+2.7\text{ V}$ vs. NHE) [36] both are more negative than those of Ag_3PO_4 . It has been reported that the oxygen vacancy on $\text{TiO}_2\text{-OV}$ can promote the visible light absorption (Fig. 3). [37] In general, the photo-generated electrons resulting from $\text{TiO}_2\text{-OV}$ would migrate to the conduction band (CB) of Ag_3PO_4 and the holes generated from Ag_3PO_4 would transfer to the valence band (VB) of $\text{TiO}_2\text{-OV}$ due to the band potential matching between Ag_3PO_4 and $\text{TiO}_2\text{-OV}$. In this case, the electrons in the CB of Ag_3PO_4 and the holes in VB of $\text{TiO}_2\text{-OV}$ were both effective for the degradation of organic dyes. However, the conduction band potential of Ag_3PO_4 ($+0.45\text{ V}$ vs. NHE) is not negative enough for the generation of $\text{O}_2^{\bullet-}$ radicals' ($+0.13\text{ V}$ vs. NHE) [15]. So the above mechanism cannot be explain the fact that $\text{O}_2^{\bullet-}$ is the major active species in a photocatalytic dye degradation system.

Based on the above analysis, a direct Z-scheme photocatalytic mechanism [38,39] with metallic Ag nanoparticles as the charge transmission relay was proposed to explain the enhanced photocatalytic activity of $\text{Ag}_3\text{PO}_4/\text{TiO}_2\text{-OV}$. As shown in Fig. 8, there are two photogenerated electron-hole transmission routes in the visible-light-driven $\text{Ag}_3\text{PO}_4/\text{TiO}_2\text{-OV}$ Z-scheme system. One route is the shifting of electrons in the conduction band of Ag_3PO_4 to metallic Ag. Due to the potential of Ag_3PO_4 the conduction band is more negative than the Fermi level of metallic Ag. Simultaneously, the holes in the valence band of $\text{TiO}_2\text{-OV}$ can migrate to the metallic Ag and combine with the electrons from Ag_3PO_4 . In a second route, the electrons photogenerated in $\text{TiO}_2\text{-OV}$ could reduce O_2 to $\text{O}_2^{\bullet-}$ through the one electron reduction process ($\text{O}_2 + \text{e}^- \rightarrow \text{O}_2^{\bullet-}$),

while holes in the valence band of Ag_3PO_4 have strong oxidation ability and can oxidize Rh B directly. In this mechanism, the photo-generated charges can be separated effectively, thus improving the photocatalytic activities of $\text{Ag}_3\text{PO}_4/\text{TiO}_2\text{-OV}$ composites. The PO_4^{3-} ions with large negative charges in Ag_3PO_4 prefer to attract holes and repel electrons. The direct Z-scheme can explain the enhanced activity of the visible-light-driven $\text{Ag}_3\text{PO}_4/\text{TiO}_2\text{-OV}$ composite system.

The stronger charge separation and migration capacity of $\text{Ag}_3\text{PO}_4/\text{TiO}_2\text{-OV}$ nanocomposite can be proved by the enhanced photocurrent under visible light irradiation. As shown in Fig. 9a, the photocurrent of $\text{Ag}_3\text{PO}_4/\text{TiO}_2\text{-OV}$ was much higher than that of the pure Ag_3PO_4 and $\text{TiO}_2\text{-OV}$ under the same condition. This result indicates that the combination of Ag_3PO_4 and $\text{TiO}_2\text{-OV}$ was able to facilitate the photoinduced charge migration efficiency. Photoluminescence (PL) emission is resulted from the recombination of free charges. The efficiency of photogenerated electrons and holes of $\text{TiO}_2\text{-OV}$, Ag_3PO_4 and $\text{Ag}_3\text{PO}_4/\text{TiO}_2\text{-OV}$ was also measured using PL analysis (Fig. 9b). It can be seen that the PL emission of Ag_3PO_4 at about 510 nm in $\text{Ag}_3\text{PO}_4/\text{TiO}_2\text{-OV}$ has been significantly quenched. The PL emission of $\text{TiO}_2\text{-OV}$ at 400–500 nm is also dramatically weakened for $\text{Ag}_3\text{PO}_4/\text{TiO}_2\text{-OV}$. A lower PL intensity indicates enhanced inhibition of the recombination of photogenerated electrons and holes, which resulted in improved photocatalytic degradation performance of the catalyst. The results of photocurrent and PL agree well indicating that the loading of Ag_3PO_4 on $\text{TiO}_2\text{-OV}$ can significantly increase the separation efficiency of photogenerated electron-hole pairs in $\text{Ag}_3\text{PO}_4/\text{TiO}_2\text{-OV}$.

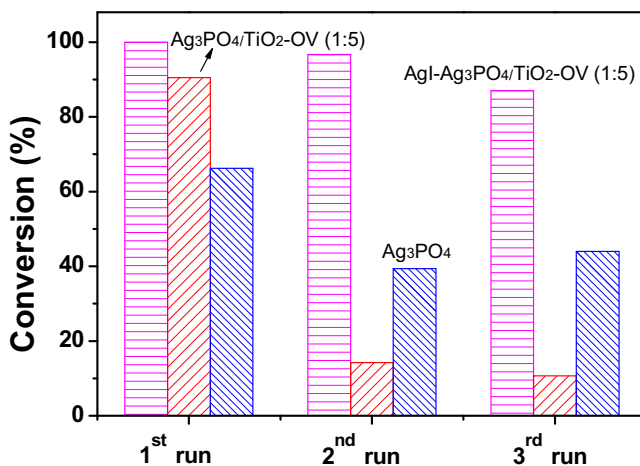


Fig. 10. Comparison of lifespans of AgI-Ag₃PO₄/TiO₂-OV (1:5), Ag₃PO₄/TiO₂-OV (1:5) and Ag₃PO₄ photocatalysts for the degradation of aqueous Rh B solution under visible light irradiation. The light irradiation time for each run is 16 min.

composites. This result is in consistent with the proposed Z-scheme mechanism of Ag₃PO₄/TiO₂-OV system.

3.5. Cycling experiments

The photocatalytic stability of Ag₃PO₄/TiO₂-OV (1:5) was investigated by collecting the used sample after photocatalysis and performing the repeated experiments of the photocatalyst under the same conditions. It is noted that the photocatalytic activity of the Ag₃PO₄/TiO₂-OV decreased noticeably from 90.5% to 10.7% of Rh B degradation after 3 recycling runs (Fig. 10). In contrast, the photocatalytic activities of Ag₃PO₄ decrease only from 66.4% to 44% of Rh B degradation after the same 3 recycling runs. These results indicate that although Ag₃PO₄/TiO₂-OV (1:5) composite has a much higher initial photocatalytic activity than that of pure Ag₃PO₄ under visible light irradiation, the stability of Ag₃PO₄/TiO₂-OV composites is less than that of Ag₃PO₄. This phenomenon may be attributed to the very fine Ag₃PO₄ particles on the surface of TiO₂-OV. As shown in the TEM images, the average diameter of Ag₃PO₄ particles loaded on TiO₂-OV ranges from 2.6 to 5.5 nm. In contrast, the average diameter of the prepared pure Ag₃PO₄ is approximately 250 nm. When Ag₃PO₄ particles are too small, the stability of Ag₃PO₄ decreases, leading to the activity loss of the Ag₃PO₄/TiO₂-OV photocatalyst. Ag₃PO₄ has a relatively high solubility in aqueous solution (0.02 g/L), [8] which results in the reduction of its stability during the photocatalytic process. Reducing Ag₃PO₄ particle size will facilitate Ag₃PO₄ to dissolve in a pholyte resulting in the increased instability of Ag₃PO₄. We have carried out a preliminary experiment that shows that the photocatalytic stability of Ag₃PO₄/TiO₂-OV could be greatly improved by in-situ depositing AgI thin layers over Ag₃PO₄ to form an AgI-Ag₃PO₄/TiO₂-OV composite system (Fig. 10). The deposition of AgI was achieved by using an in-situ anion-exchange method. [8,20] Since AgI possesses a much lower solubility (3.1×10^{-5} g/L) than that of Ag₃PO₄, [8] the lower solubility and higher resistance to corrosion of AgI improves the stability of Ag₃PO₄ nanoparticles and thus the stability of the Ag₃PO₄/TiO₂-OV system. This study is still in progress. The control and optimization of Ag₃PO₄ particle sizes and stability improvement will be reported in the next phase of this research.

4. Conclusions

Ultrafine Ag₃PO₄ nanoparticles with an average particle size ranging from 2.6 to 5.5 nm were successfully prepared on the

surface of an oxygen vacated TiO₂ (TiO₂-OV) support. A facile in-situ chemical deposition method is applied for this synthesis. The prepared Ag₃PO₄/TiO₂-OV composites exhibit an enhanced photocatalytic activity compared to that of pure Ag₃PO₄ or Ag₃PO₄/TiO₂ photocatalysts for the photocatalytic degradation of both aqueous Rh B and phenol solutions. Results show that a 3.4 times reaction rate increase has been achieved with an 49% Ag loading reduction for Ag₃PO₄/TiO₂-OV photocatalyst as compared with pure Ag₃PO₄ catalyst. The quenching effects of different scavengers suggest that the reactive hole (h^+) scavenger and O₂^{•-} free radicals play major roles in the Rh B degradation. However, stability testing has shown that the photocatalytic activity of the Ag₃PO₄/TiO₂-OV decreased noticeably after three reaction recycles, indicating that although very high initial activity and cost effectiveness for ultrafine Ag₃PO₄ nanoparticles on a TiO₂-OV support can be achieved, the very fine Ag₃PO₄ nanoparticles reduce the lifespan of Ag₃PO₄/TiO₂-OV photocatalysts. The result from a preliminary experiment has indicated that the stability of Ag₃PO₄/TiO₂-OV can be extensively improved by in-situ depositing AgI thin layers over Ag₃PO₄. Optimization of Ag₃PO₄ particle sizes and loading amounts will be a critical task for this research before possible commercialization of Ag₃PO₄/TiO₂-OV photocatalysts.

Acknowledgments

This work was financially supported by the Shanghai Key Project for Fundamental Research (13JC1402800), the "Dawn" Program of Shanghai Education Commission (11SG52) and Science and Technology Commission of Shanghai Municipality (14DZ22261000). The invaluable support of all the above funding agents is greatly appreciated. Yang Li and Peifu Wang contributed equally to this study and share first authorship.

Appendix A. Supplementary data

Supplementary data associated with this article can be found, in the online version, at <http://dx.doi.org/10.1016/j.apcatb.2016.12.059>.

References

- [1] X. Chen, S. Shen, L. Guo, S.S. Mao, Chem. Rev. 110 (2010) 6503–6570.
- [2] A.L. Linsebigler, G. Lu, J.T. Yates, Chem. Rev. 95 (1995) 735–758.
- [3] P. Wang, B. Huang, X. Qin, X. Zhang, Y. Dai, J. Wei, M.H. Whangbo, Angew. Chem. Int. Engl. 47 (2008) 7931–7933.
- [4] J. Yu, G. Dai, B. Huang, J. Phys. Chem. C 113 (2009) 16394–16401.
- [5] P. Wang, B. Huang, X. Zhang, X. Qin, H. Jin, Y. Dai, Z. Wang, J. Wei, J. Zhan, S. Wang, J. Wang, M.H. Whangbo, Chem. Eur. J. 15 (2009) 1821–1824.
- [6] Y. Bi, S. Ouyang, N. Umezawa, J. Cao, J. Ye, J. Am. Chem. Soc. 133 (2011) 6490–6492.
- [7] Z. Yi, J. Ye, N. Kikugawa, T. Kako, S. Ouyang, H. Stuart-Williams, H. Yang, J. Cao, W. Luo, Z. Li, Y. Liu, R.L. Withers, Nat. Mater. 9 (2010) 559–564.
- [8] Y. Bi, S. Ouyang, J. Cao, J. Ye, Phys. Chem. Chem. Phys. 13 (2011) 10071–10075.
- [9] Z. Lou, B. Huang, Z. Wang, X. Ma, R. Zhang, X. Zhang, X. Qin, Y. Dai, M.-H. Whangbo, Chem. Mater. 26 (2014) 3873–3875.
- [10] C. Cui, S. Li, Y. Qiu, H. Hu, X. Li, C. Li, J. Gao, W. Tang, Appl. Catal. B-Environ. 200 (2017) 666–672.
- [11] L. Liu, Y. Qi, J. Lu, S. Lin, W. An, Y. Liang, W. Cui, Appl. Catal. B-Environ. 183 (2016) 133–141.
- [12] S. Kumar, T. Surendar, A. Baruah, V. Shanker, J. Mater. Chem. A 1 (2013) 5333.
- [13] Y. Hongjian, Y. Yong, L. Jianghao, M. Peiyan, W. Yucheng, Z. Fan, F. Zhengyi, J. Mater. Chem. A 3 (2015) 19439–19444.
- [14] L. Liu, L. Ding, Y. Liu, W. An, S. Lin, Y. Liang, W. Cui, Appl. Catal. B-Environ. 201 (2017) 92–104.
- [15] P. Tan, X. Chen, L. Wu, Y.Y. Shang, W. Liu, J. Pan, X. Xiong, Appl. Catal. B-Environ. 202 (2017) 326–334.
- [16] T. Yan, J. Tian, W. Guan, Z. Qiao, W. Li, J. You, B. Huang, Appl. Catal. B-Environ. 202 (2017) 84–94.
- [17] Y. Chang, K. Yu, C. Zhang, R. Li, P. Zhao, L.-L. Lou, S. Liu, Appl. Catal. B-Environ. 176–177 (2015) 363–373.
- [18] Q. Wu, P. Wang, F. Niu, C. Huang, Y. Li, W. Yao, Appl. Surf. Sci. 378 (2016) 552–563.

- [19] Q. Wu, P. Wang, F. Niu, Y. Hong, M. Luo, W. Yao, J. Taiwan Inst. Chem. Eng. 60 (2016) 532–537.
- [20] Z. Chen, W. Wang, Z. Zhang, X. Fang, J. Phys. Chem. C 117 (2013) 19346–19352.
- [21] W.F. Yao, B. Zhang, C.P. Huang, C. Ma, X.L. Song, Q.J. Xu, J. Mater. Chem. 22 (2012) 4050–4055.
- [22] X. Pan, Y.-J. Xu, J. Phys. Chem. C 117 (2013) 17996–18005.
- [23] X. Pan, Y.-J. Xu, Appl. Catal. A: Gen. 459 (2013) 34–40.
- [24] X. Pan, M.Q. Yang, X. Fu, N. Zhang, Y.J. Xu, Nanoscale 5 (2013) 3601–3614.
- [25] X. Pan, N. Zhang, X. Fu, Y.-J. Xu, Appl. Catal. A: Gen. 453 (2013) 181–187.
- [26] H. Katsumata, M. Taniguchi, S. Kaneko, T. Suzuki, Catal. Commun. 34 (2013) 30–34.
- [27] X.J. Chen, Y.Z. Dai, X.Y. Wang, J. Guo, T.H. Liu, F.F. Li, J. Hazard. Mater. 292 (2015) 9–18.
- [28] R. Li, H. Kobayashi, J. Guo, J. Fan, Chem. Commun. 47 (2011) 8584–8586.
- [29] P. Wang, B. Huang, X. Zhang, X. Qin, Y. Dai, Z. Wang, Z. Lou, ChemCatChem 3 (2011) 360–364.
- [30] X. Xiao, L. Ge, C. Han, Y. Li, Z. Zhao, Y. Xin, S. Fang, L. Wu, P. Qiu, Appl. Catal. B-Environ. 163 (2015) 564–572.
- [31] Z. Zheng, B. Huang, X. Qin, X. Zhang, Y. Dai, M.-H. Whangbo, J. Mater. Chem. 21 (2011) 9079.
- [32] G. Xi, J. Ye, Q. Ma, N. Su, H. Bai, C. Wang, J. Am. Chem. Soc. 134 (2012) 6508–6511.
- [33] H. Zhang, X. Lv, Y. Li, Y. Wang, J. Li, ACS Nano 4 (2009) 380–386.
- [34] H. Zhang, H. Huang, H. Ming, H. Li, L. Zhang, Y. Liu, Z. Kang, J. Mater. Chem. 22 (2012) 10501–10506.
- [35] Y. Xu, M.A.A. Schoonen, Am. Mineral. 85 (2000) 543–556.
- [36] N. Serpone, P. Maruthamuthu, P. Pichat, E. Pelizzetti, H. Hidaka, J. Photochem. Photobiol. A: Chem. 85 (1995) 247–255.
- [37] A. Naldoni, M. Allieta, S. Santangelo, M. Marelli, F. Fabbri, S. Cappelli, C.L. Bianchi, R. Psaro, V. Dal Santo, J. Am. Chem. Soc. 134 (2012) 7600–7603.
- [38] H. Tada, T. Mitsui, T. Kiyonaga, T. Akita, K. Tanaka, Nat. Mater. 5 (2006) 782–786.
- [39] J. Jin, J. Yu, D. Guo, C. Cui, W. Ho, Small 11 (2015) 5262–5271.